# Observation of the dominant spin-triplet supercurrent in Josephson spin valves with strong Ni ferromagnets

O. M. Kapran,[1] A. Iovan,[1] T. Golod,[1] and V. M. Krasnov[1,2,*]

[1]*Department of Physics, Stockholm University, AlbaNova University Center, SE-10691 Stockholm, Sweden*

[2]*Moscow Institute of Physics and Technology, State University, 9 Institutskiy per., Dolgoprudny, Moscow Region 141700, Russia*

(Received 24 November 2019; accepted 3 January 2020; published 18 February 2020)

We study experimentally nanoscale Josephson junctions and Josephson spin valves containing strongly ferromagnetic Ni interlayers. We observe that in contrast to junctions, spin valves with the same geometry exhibit anomalous $I_c(H)$ patterns with two peaks separated by a dip. We develop several techniques for *in situ* characterization of micromagnetic states in our nanodevices, including magnetoresistance, absolute Josephson fluxometry, and first-order-reversal-curves analysis. They reveal a clear correlation of the dip in supercurrent with the antiparallel state of a spin valve and the peaks with two noncollinear magnetic states, thus providing evidence for generation of spin-triplet superconductivity. A quantitative analysis, based on micromagnetic simulations, brings us to the conclusion that the triplet current in our Ni-based spin valves is approximately three times larger than the conventional spin-singlet supercurrent.

DOI: 10.1103/PhysRevResearch.2.013167

## I. INTRODUCTION

Spin-polarized ferromagnetism is antipathetic to spin-singlet superconductivity. However, destruction of singlet Cooper pairs in a ferromagnet is not an instant process. Pairing correlations survive over a certain time/distance, during which the precession of spins in an exchange field may create a correlated triplet pair. The corresponding odd-frequency spin-triplet order parameter has been predicted theoretically using various approaches [1–16]. This inspired an intense experimental search for this exotic state in superconductor/ferromagnet (S/F) heterostructures [17–29]. Although supercurrents through F were reported many times [17–28], it is difficult to prove their triplet nature. First, even spin-singlet current can flow over long ranges in clean or weak ferromagnets [1,5,10,30]. The singlet current is reduced in strong F, which should be materials of choice for a critical test. Second, the supercurrent strongly depends on a usually unknown domain structure in F [20,27,31], flux quantization in S [32,33], both influenced by size and geometry. This uncertainty can be obviated in nanoscale devices with mono- (or few) domain F layers and with the flux-quantization field larger than the coercive field [32]. Finally, the long-range triplet current should appear only in the noncollinear magnetic state [2,6–10]. Therefore, unambiguous identification of the pairing order is only possible if the micromagnetic state of the actual device is known. It is not sufficient to analyze similar large-area heterostructures because their magnetic properties (coercive fields, domain structure, shape anisotropy) would be different from a nanodevice. To prove (disprove) the triplet nature of supercurrent, it is necessary to demonstrate its correlation (anticorrelation) with the noncollinear state [19–21,24–28]. In the end, it is all about having an *in situ* control over the micromagnetic state of the studied nanodevice. This is the main motivation of our work.

The noncollinear magnetic state can be controllably created in monodomain spin valves. The simplest is the pseudospin valve $F_1NF_2$ with two $F_{1,2}$ layers separated by a normal metal (N) spacer. The spin-triplet current in this case is second-harmonic with respect to the phase difference and is proportional to the difference between $F_1$ and $F_2$ [8–10,13,14,16] (see the Appendix for more details). Therefore, an asymmetric spin valve $F_1 \neq F_2$ is needed for generation of the triplet current. The asymmetry (different coercive fields) is also needed for controllable tuning of the relative magnetization angle $\alpha$ between $F_{1,2}$ layers.

Here we study experimentally nanoscale SFS Josephson junctions (JJ's) and $SF_1NF_2S$ Josephson spin valves (JSV's). We use strong F (Ni) to suppress singlet currents and to make triplet currents dominant. We focus on development of various methods for *in situ* characterization of micromagnetic states in our nanodevices, including magnetoresistance (MR), absolute Josephson fluxometry (AJF), and first-order-reversal-curves (FORC) analysis. We observe that JSV's behave qualitatively differently compared to JJ's with similar geometry: they exhibit non-Fraunhofer $I_c(H)$ modulation with two distinct peaks separated by a dip. *In situ* characterization reveals a clear correlation of the supercurrent dip with the antiparallel (AP) state of the JSV and the peaks with two noncollinear states around it. This provides *in situ* evidence for the generation of spin-triplet superconductivity.

*Vladimir.Krasnov@fysik.su.se

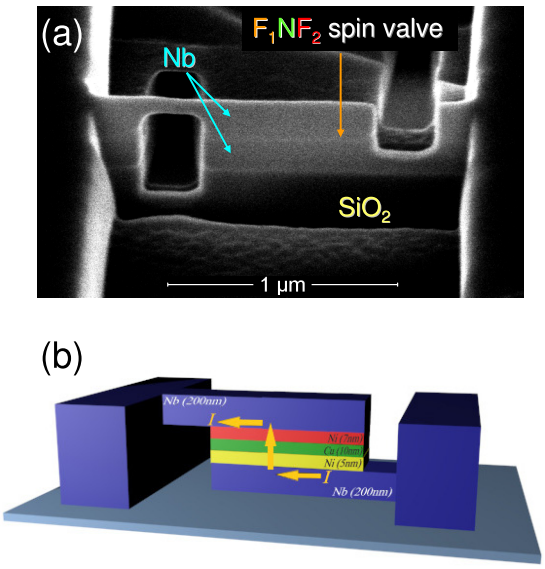


FIG. 1. (a) SEM image of one of the studied Josephson spin valves. (b) A clarifying sketch of the device. Arrows indicate the zigzag current flow path. The transport current is sent along the bridge, but, because of the two FIB cuts, it is forced to flow across F-layers.

## II. EXPERIMENT

We study nanoscale Nb(200 nm)/Ni(5 nm)-Cu(10 nm)-Ni(7 nm)/Nb(200 nm) JSV's and Nb(200 nm)/Ni (5–10 nm)/Nb(200 nm) JJ's. Thin-film multilayers are deposited by dc-magnetron sputtering and patterned into $\mu$m-sized bridges by photolithography and reactive ion etching. Subsequently they are transferred into a dual-beam scanning electron microscope (SEM)/focused ion beam (FIB) and nanoscale devices are made by three-dimensional (3D) FIB nanosculpturing [20,34]. Both JJ's and JSV's have similar rectangular shapes with short sides 100–300 nm and long sides 250–1400 nm. Several devices with different sizes are made at the same chip. Figure 1 shows a SEM image of one of the studied JSV's with a clarifying sketch.

Measurements are performed in closed-cycle cryostats. For analysis of $I_c(H)$ modulation, the in-plane magnetic field is applied either parallel ($H_\parallel$, along the easy magnetization axis) or perpendicular ($H_\perp$, along the hard axis) to the long side. More details can be found in the Supplemental Material [35].

## III. PROPERTIES OF SFS JUNCTIONS

Figures 2(a) and 2(b) represent measured $I_c(H_\parallel)$ patterns in the easy-axis orientation for JJ's (a) Ni (5 nm) with area 164 × 896 nm$^2$, and (b) Ni (7 nm) with areas 200 × 1000 nm$^2$. Figure 2(c) shows $I_c(H_\perp)$ along the hard axis for the same Ni (5 nm) JJ. Up and down field sweeps are shown. They exhibit hysteresis due to finite coercivity. From Figs. 2(a) and 2(b) it can be seen that the hysteresis starts/ends at about $\sim \pm 1.5$ kOe, which represents the saturation field. In all cases SFS JJ's exhibit Fraunhofer-type $I_c(H)$ modulation with a single central maximum [36]. This indicates a good uniformity of Ni interlayers [37].

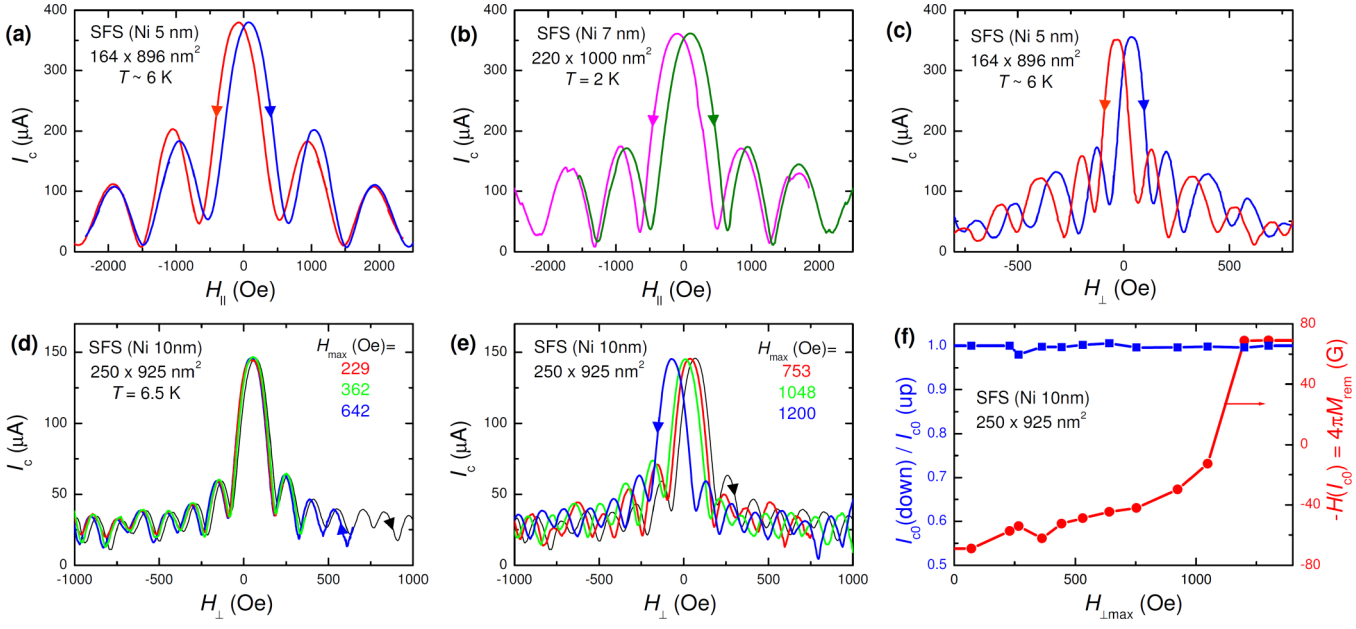


FIG. 2. Characteristics of SFS (Nb/Ni/Nb) Josephson junctions with different Ni thicknesses. (a) and (b) $I_c(H_\parallel)$ patterns for up and down field sweeps for junctions with (a) 5 nm and (b) 7 nm Ni thickness in field parallel to the long side. (c) $I_c(H_\perp)$ modulation for the same Ni (5 nm) junction in the field perpendicular to the long side. Note that $I_c(H)$ has Fraunhofer-type modulation at both field orientations. (d)–(f) First-order-reversal-curves analysis of $I_c(H_\perp)$ patterns for a junction with Ni (10 nm). Black curves in (d) and (e) represent the upward sweep from the saturated negative state. Red, green, and blue curves represent reversal curves with different $H_{\max}$. (f) The summary of FORC analysis from (d) and (e). Red circles (right axis) show the position of the central maximum, representing the remnant magnetization in the junction. Blue squares (left axis) show the amplitude of the central peak. It is seen that remagnetization of the SFS junction leads to a trivial hysteresis: the $I_c(H)$ patterns maintain their shapes and merely shift due to changing magnetization of the F interlayer.

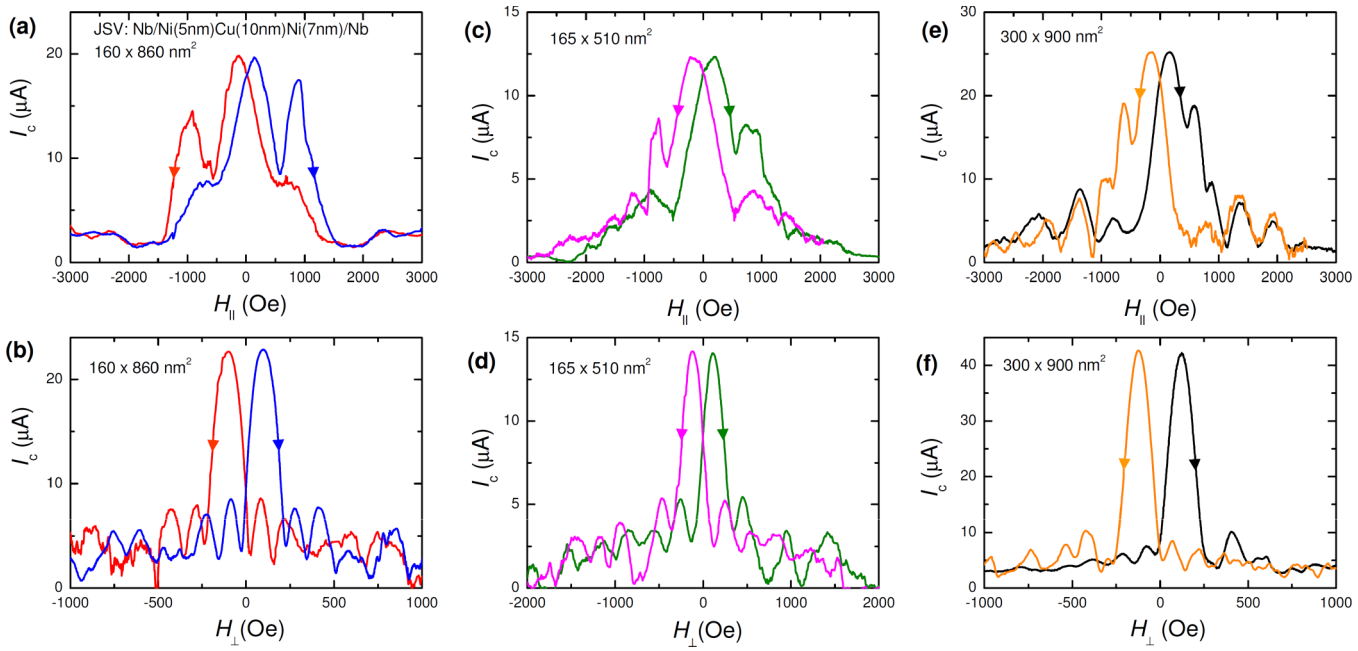


FIG. 3. $I_c(H)$ modulation patterns for three Josephson spin valves with different sizes, made at the same chip. Parts (a),(c),(e) in fields parallel and (b),(d),(f) perpendicular to the long side. (a),(b) JSV 160 × 860 nm$^2$ at $T \simeq 2$ K; (c),(d) JSV 165 × 510 nm$^2$ at $T \simeq 2$ K; (e),(f) JSV 300 × 900 nm$^2$ at $T \simeq 0.6$ K. Note non-Fraunhofer double-peak patterns in a parallel field orientation.

### A. First-order-reversal-curves analysis

FORC is a powerful tool for *in situ* characterization of magnetic states in complex ferromagnetic structures [38–40]. The analysis starts at the same saturated state. Then the field is swept to a reversal field $H_{\max}$, and measurements are carried out on the way back to the saturated state. Figures 2(d) and 2(e) represent $I_c(H_\perp)$ FORC's for a JJ with Ni (10 nm). Thin black lines represent the upward sweep from the saturated $\downarrow\downarrow$ state. Red, green, and blue lines are FORCs with different $H_{\perp\max}$. FORC's show very little hysteresis up to $H_{\perp\max} \sim 1.1$ kOe and then rapidly jump to the saturated $\uparrow\uparrow$ state. This reflects an abrupt remagnetization of the Ni nanoparticle within the JJ. Note that the curves for different $H_{\perp\max}$ in Figs. 2(d) and 2(e) maintain the same Fraunhofer-type shape, which just shifts upon remagnetization of the Ni interlayer.

### B. Absolute Josephson fluxometry

AJF is based on flux quantization in Josephson devices, due to which minima and maxima of $I_c$ occur at integer and half-integer flux quanta $\Phi_0$ within a device. Magnetization is related to flux via $M = (\Phi/Ld^* - H)/4\pi$, where $L$ is the size and $d^*$ the magnetic thickness of the device. Thus absolute values of $M$ can be obtained at discrete fields determined by the flux quantization field $\Delta H = \Phi_0/Ld^*$ [20,41].

### C. Combined AJF+FORC

For nanodevices with small $L$ and large $\Delta H$ the discreteness of AJF is a limitation. To obviate this problem, we combine AJF with FORC, which allows continuous determination of $M(H_{\max})$ for arbitrarily small devices. For example, the central maxima of FORC's in Figs. 2(d) and 2(e) correspond to $\Phi = 0$. Therefore, fields at which they occur, $H(I_{c0})$, represent absolute values of remnant magnetization, $M_{\rm rem} = -H(I_{c0})/4\pi$. Since we can vary $H_{\max}$ with arbitrarily small steps, we can get a continuous $M_{\rm rem}(H_{\max})$ curve from such AJF+FORC analysis even for very small devices. This is demonstrated in Fig. 2(f), where red circles represent $-H(I_{c0}) = M_{\rm rem}/4\pi$ as a function of $H_{\perp\max}$ for FORC's from Figs. 2(d) and 2(e). It is seen that $M_{\rm rem}$ switches rapidly at $H_{\perp\max} \gtrsim 1.1$ kOe, which represents the coercive field. Blue squares represent $I_{c0}$, which apparently stays constant. Thus, hysteresis in SFS JJ's is *trivial*: remagnetization of the F layer changes the internal flux, which just shifts $I_c(H)$ patterns without changing their shapes.

## IV. PROPERTIES OF JOSEPHSON SPIN VALVES

Figure 3 shows $I_c(H)$ patterns for three JSV's with different sizes from the same chip in easy- [Figs. 3(a), 3(c), and 3(e)] and hard- [Figs. 3(b), 3(d), and 3(f)] axis orientations. In stark contrast to SFS JJ's [Figs. 2(a) and 2(b)], JSV's with a similar geometry exhibit a profound distortion of the central $I_c(H)$ maximum in the easy-axis orientation. The distortion depends on the size. For the narrowest JSV's, (a) $L = 160$/nm, the central maximum splits into two peaks, separated by a dip. With increasing JSV size, (e) $L = 300$ nm, the splitting decreases. For the hard-axis orientation, corresponding to larger sizes: (d) 510 nm, (b) 860 nm, and (f) 900 nm, the distortion seemingly disappears and $I_c(H)$ patterns acquire Fraunhofer-type shapes. The latter indicates good uniformity of the barrier [37]. Therefore, the double-peak distortion in the easy-axis orientation *for the same devices* cannot be ascribed to nonuniformity or defects. This is our central observation that we will analyze below.

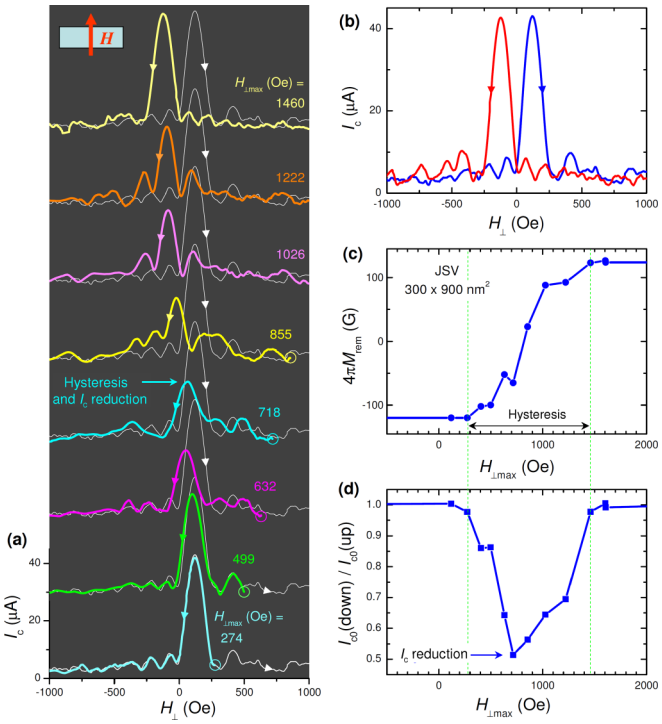


FIG. 4. Experimental FORC analysis for a JSV 300 × 900 nm$^2$ in the hard-axis orientation at $T = 1.0$ K. (a) Thin white lines represent $I_c(H_\perp)$ for the upward field sweep starting from the saturated ↓↓ state. Thick color lines are reversal curves starting from different $H_{\perp max}$. The curves are shifted vertically for clarity. $H_{\perp max}$ are indicated by circles and/or text. (b) Mirror-symmetric $I_c(H_\perp)$ curves for upward (blue) and downward (red) field sweeps from saturated ↓↓ and ↑↑ states. (c) Position of the central maximum of $I_c(H_\perp)$ FORC's as a function of the reversal field $H_{\perp max}$. It represents absolute values of remnant magnetization of the JSV. (d) Amplitudes of the central maximum of downward FORC's $I_{c0}$ (down), normalized by that for the upward sweep $I_{c0}$ (up) as a function of the reversal field $H_{\perp max}$. Note that in contrast to SFS junctions, Fig. 2(f), remagnetization of the JSV leads to a nontrivial hysteresis, which is accompanied by a significant reduction of the supercurrent.

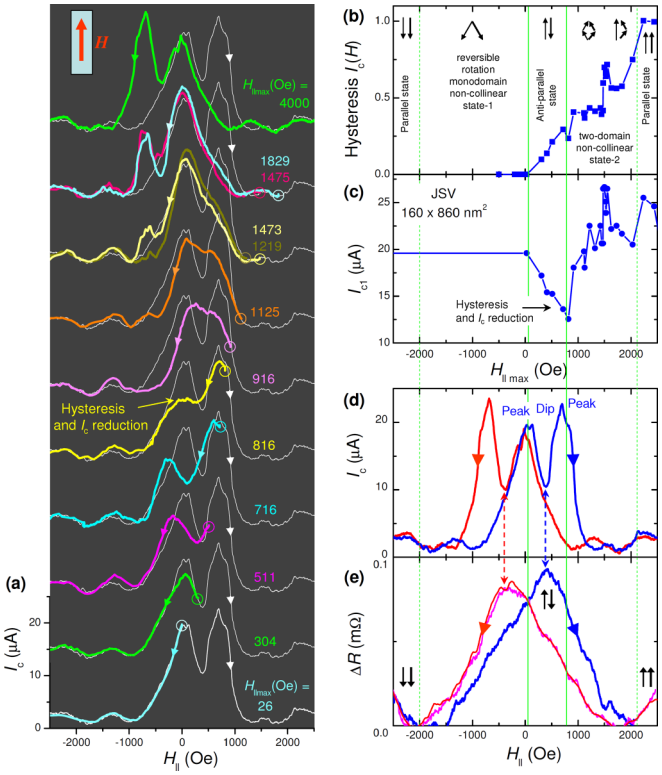


FIG. 5. *In situ* characterization of a JSV 160 × 860 nm$^2$ in the easy-axis orientation at $T = 1.2$ K. (a) Experimental FORC's (thick color lines) for different $H_{\parallel max}$, indicated by circles. The curves are shifted vertically for clarity. (b) Hysteresis of $I_c(H)$, equal to the area between upward and reversal curves in (a). (c) Amplitude of the first supercurrent peak $I_{c1}(H \sim 0)$. Arrows in the top of panel (b) depict the magnetic state of the JSV, as described in the text. (d) $I_c(H_\parallel)$ patterns for upward (blue) and downward (red) field sweeps from saturated ↓↓ and ↑↑ states. (e) Spin-valve magnetoresistance, measured at bias current much larger than $I_c$. Dashed vertical arrows in (d),(e) indicate a clear correlation between the dip in $I_c$ and the maximum of MR, corresponding to the AP state of the spin valve.

### A. Hard-axis orientation

We start with the hard-axis orientation because in this case $I_c(H_\perp)$ patterns have Fraunhofer-type shapes facilitating similar analysis as for SFS junctions. Figure 4(a) represents $I_c(H_\perp)$ FORC's for a JSV 300 × 900 nm$^2$. Thin white lines represent the upward sweep and thick color lines the FORC's with different $H_{\perp max}$. The lower curve indicates that up to the end of the central peak, $H_{\perp max} \lesssim 274$ Oe, FORC's are fully reversible. Above it a hysteresis appears. However, in contrast to SFS JJ's [see Fig. 2(e)], the hysteresis is *nontrivial*: Remagnetization of JSV's leads to *both* the shift and distortion of $I_c(H)$ patterns. In particular, it leads to a significant reduction of the central maximum, $I_{c0}$, which reaches a minimum at $H_{\perp max} \simeq 718$ Oe. With a further increase of $H_{\perp max}$, $I_{c0}$ grows back and recovers to the original value when $H_{\perp max}$ exceeds the saturation field; see Fig. 4(b). Figures 4(c) and 4(d) represent AJF+FORC analysis: (c) $M_{rem}(H_{\perp max})$ and (d) $I_{c0}(H_{\perp max})$. It is seen that $I_{c0}$ is reduced by up to a factor 2 within the hysteresis region, marked by vertical lines. It demonstrates that the hysteresis for JSV's is nontrivial, compared to that for SFS junctions; see Fig. 2(f).

### B. Easy-axis orientation

In Fig. 5 we analyze the behavior of the 160 × 860 nm$^2$ JSV's in the easy-axis orientation. Figure 5(a) represents FORC analysis. FORC's are reversible until $H_{\parallel max}$ passes the first $I_c(H_\parallel)$ peak in the upward sweep (thin white lines). At higher fields hysteresis appears, accompanied by the reduction of $I_c$. The $I_c$ reaches a minimum when $H_{\parallel max}$ passes the second maximum at 816 Oe. At $H_{\parallel max} = 916$–1473 Oe, a state with one dominant peak is observed. With a further increase of $H_{\parallel max} \geqslant 1475$ Oe, the second peak reemerges. Finally, for $H_{\parallel max}$ larger than the saturation field, $\simeq 2$ kOe, the reversal curve becomes mirror-symmetric with respect to the upward curve. Thus, hysteresis in JSV's is nontrivial for both field orientations: the appearance of hysteresis is always accompanied by the reduction of supercurrent, as indicated in Figs. 4(d) and 5(c).

### C. Difference between SFS junctions and JSV's

To understand the difference in the behavior of JJ's and JSV's, we first note that the conventional Fraunhofer $I_c(H)$ modulation in JJ's occurs due to flux quantization with field-independent critical current density, $J_c(H) = \text{const}$. The observed trivial hysteresis in SFS junctions suggests that upon remagnetization of a single F layer, only the total flux changes, but $J_c$ remains unchanged. Conversely, the nontrivial hysteresis in JSV's indicates that $J_c$ is not constant, but depends on the relative orientation $\alpha$ of the two F layers. It is anticipated [8–10,32] that the triplet component should vanish in the collinear $\alpha = 0^\circ, 180^\circ, 360^\circ$ states and should have maxima in the noncollinear $\alpha = 90^\circ, 270^\circ$ states; see the numerical analysis in the Appendix.

The origins of magnetic hysteresis in JJ's and JSV's are also different. For JJ's with a single F layer, it is caused predominantly by the shape anisotropy. The presence of the second F layer in JSV's leads to another mechanism caused by magnetostatic interaction between $F_{1,2}$ layers, which favors the AP state. In a monodomain case, remagnetization of a JSV starts by a scissorlike rotation of $M_{1,2}$ [32]. Such rotation is reversible and nonhysteretic. It continues until the softer $F_1$ layer flips and JSV switches into the AP state. Magnetostatic stability of the AP state leads to the appearance of hysteresis: if the field is reversed, the spin valve will remain in the AP state. With increasing field, the harder $F_2$ layer also flips and JSV enters into the second scissorlike noncollinear state, which gradually turns into the parallel $\uparrow\uparrow$ state [32]. Micromagnetic simulations for our JSV's, presented in the Appendix, confirm such a behavior but also demonstrate that remagnetization may involve the formation of two domains. Few domains do not change the overall picture, but they lead to additional hysteresis associated with the disappearance of each domain wall.

To summarize the above discussion, the principal difference between JJ's and JSV's is in $J_c(H)$ dependence, which is constant for JJ's and depends on magnetization orientation, $J_c[\alpha(H)]$, for JSV's. During remagnetization $\alpha(H)$ varies from $0^\circ$ to $360^\circ$ passing two times through noncollinear states $\alpha = 90^\circ$ and $270^\circ$. Therefore, the triplet component should have two peaks at $\alpha = 90^\circ$ and $270^\circ$, surrounding a dip in the AP state $\alpha = 180^\circ$, while the singlet component should have one sharp maximum in the AP state; see the Appendix. This provides a robust qualitative test for the nature of the dominant supercurrent: Since the appearance of hysteresis in JSV is caused by the switching from the noncollinear scissor state to the collinear AP state, the associated change in $I_c$ should unambiguously reveal the dominant type of supercurrent. If $I_c$ increases, then it is singlet, and if it decreases, it is triplet. The latter is qualitatively consistent with our observations; see Figs. 4(d) and 5(c).

### D. *In situ* characterization of the JSV state

Unambiguous confirmation of the triplet nature of supercurrent requires detailed knowledge of the micromagnetic state. Figures 5(b)–5(e) represent the *in situ* analysis of the magnetic state evolution for the easy-axis orientation of the JSV. Figure 5(b) represents hysteresis, i.e., the area between upward $I_c(H_\parallel)$ and FORC's from Fig. 5(a). Figure 5(c) shows amplitudes of the first (left) main peak $I_{c1}$ in FORC's. Figure 5(e) shows high-bias spin-valve magnetoresistance measured at the same device [35]. Parallel and AP states of JSV correspond to minima and maxima of MR, respectively [20]. Such an analysis provides a self-consistent understanding of the magnetic state evolution in the JSV. The saturation field, at which FORC's stop changing [see Fig. 5(b)] and MR reaches minimum [see Fig. 5(e)], is $\sim \pm 2$ kOe. At $H < -2$ kOe, the JSV is in the $\downarrow\downarrow$ parallel state $\alpha \simeq 0$. In a broad range $-2$ kOe $< H_{\parallel\max} < 26$ Oe, there is no hysteresis. Consequently, the JSV is in a monodomain noncollinear scissor state with reversible rotation $0^\circ < \alpha < 180^\circ$. Hysteresis appears at $H_{\parallel\max} \gtrsim 26$ Oe, indicating switching into the magnetostatically stabile AP state $\alpha \simeq 180^\circ$, as confirmed by the large value of MR. At $H_{\parallel\max} > 816$ Oe a sudden change occurs both in hysteresis [Fig. 5(b)] and $I_{c1}$ [Fig. 5(c)]. It indicates a switching out of the AP state into a second noncollinear state $180^\circ < \alpha < 360^\circ$. At $H_{\parallel\max} \simeq 1473$ Oe there is yet another jump in both hysteresis and $I_{c1}$ before reaching the saturated $\uparrow\uparrow$ parallel state, $\alpha = 360^\circ$, at $\sim$2 kOe. Such a two-step switching from AP to $\uparrow\uparrow$ parallel state is fully consistent with micromagnetic simulations presented in the Appendix and is due to the formation of two domains in both layers. At $H_{\parallel\max} \simeq 1473$ Oe the thinner F layer switches into the monodomain state, followed by the thicker F layer close to the positive saturation field. Arrows in the top part of Fig. 5(b) sketch the evolution of magnetic states during the remagnetization.

### E. Correlation between the supercurrent and the magnetic state in JSV

Now we can look at correlations between the supercurrent and the magnetic state. In Fig. 5(d) we show $I_c(H)$ patterns for this JSV. Let us focus on the upward field sweep (blue line). It has a double-peak structure. Solid vertical lines going through Figs. 5(b)–5(e) emphasize that all *in situ* characterization methods unanimously connect the dip with the AP state. Most straightforwardly, this is seen from a comparison with the MR. Dashed arrows in Figs. 5(d) and 5(e) indicate that the dip in $I_c$ corresponds to the maximum of MR. Furthermore, FORC analysis, Figs. 5(b) and 5(c), indicates that the field range of the primary hysteresis, $26 < H_{\parallel\max} \lesssim 816$ Oe, associated with the magnetostatic stability of the AP state coincides with the field range between the two peaks, and that the appearance of this hysteresis is accompanied by the reduction of the $I_{c1}$ peak. Consequently, entrance into the AP state leads to a significant reduction of $I_c$ through the JSV. However, the supercurrent recovers upon leaving the collinear AP state in both directions, resulting in the observed double-peak $I_c(H)$ pattern. We emphasize that such behavior is opposite to the expectations for the singlet current, which should be at maximum in the AP state and is consistent with the predictions for the odd-frequency spin-triplet supercurrent; see the Appendix.

We note that such an unusual behavior has not been reported in an earlier similar work [20] on JSV's containing diluted CuNi ferromagnets because in that case the dominant supercurrent ($\sim$80%) had a singlet nature. An estimation based on numerical fitting of our data, presented in the Appendix, indicates that in our Ni-based JSV's the triplet

current amplitude is approximately three times larger than the singlet. This helps to uncover the characteristic double-peak modulation, which provides unambiguous evidence for generation of the spin-triplet order parameter. Yet, even in Ni-based JSV's the dip in the AP state does not go to zero, indicating that there is still a significant subdominant (∼30%) singlet supercurrent even through a relatively thick Ni.

## V. CONCLUSION

To conclude, both singlet and triplet supercurrents can flow through S/F heterostructures [1–16]. The unique feature of our work that adds to further understanding of the triplet state, along with earlier experimental works [17–28], was the development of *in situ* characterization techniques for an accurate assessment of micromagnetic states in the actual nanodevices. In particular, we developed an AJF+FORC technique, a powerful tool allowing absolute magnetometry of nanodevices and accurate identification of micromagnetic states. We fabricated and studied nanoscale Josephson junctions and (pseudo) spin valves with Ni interlayers. Small sizes enabled mono- (or few) domain configurations, which could be unambiguously identified. A strong F (Ni) was employed for reduction of the singlet current, enabling the dominant triplet component. This was instrumental for observation of an extraordinary behavior of JSV's, qualitatively different from similar-sized SFS JJ's. Namely, $I_c(H)$ modulation of studied JSV's had two main peaks separated by the dip and exhibited the nontrivial hysteresis, accompanied by the reduction of $I_c$. The *in situ* characterization showed a clear correlation of the $I_c$ dip with the antiparallel state of the spin valve and the two peaks with the two noncollinear states aside from it. This provides unambiguous evidence for generation of the spin-triplet order parameter.

## ACKNOWLEDGMENTS

This work was supported by the European Union H2020-WIDESPREAD-05-2017-Twinning project "SPINTECH" under Grant Agreement No. 810144 and the Russian Science Foundation Grant No. 19-19-00594. The manuscript was written during a sabbatical semester of V.M.K. at MIPT, supported by the Faculty of Natural Sciences at SU and the Russian Ministry of Education and Science within the program "5top100."

## APPENDIX: NUMERICAL MODELING OF A JOSEPHSON SPIN VALVE

To clarify the behavior of JSV's, we perform numerical analysis. Josephson current in JSV's has three main components [10]: the short-range spin-singlet $I_{ss}$, the long-range spin singlet $I_{sl}$, and the long-range spin-triplet $I_{tr}$. Their local values depend on relative angles, $\alpha(x, y)$, between magnetizations, $M_{1,2}$, of the two F layers and the Josephson phase difference between S electrodes $\varphi(x, y)$:

$$I_{ss}(x, y) = I_{ss0}\cos^2[\alpha(x, y)/2]\sin[\varphi(x, y)], \quad \text{(A1)}$$

$$I_{sl}(x, y) = I_{sl0}\sin^2[\alpha(x, y)/2]\sin[\varphi(x, y)], \quad \text{(A2)}$$

$$I_{tr}(x, y) = I_{tr0}\sin^2[\alpha(x, y)]\sin[2\varphi(x, y)]. \quad \text{(A3)}$$

To calculate $I_c(H)$ we follow the procedure from Ref. [32]. First we perform a micromagnetic simulation in OOMMF, which provides the two-dimensional distribution of components $M_{x1,2}(x, y)$ and $M_{y1,2}(x, y)$. Next, we calculate $\varphi$ by direct integration of

$$\frac{\partial\varphi(x, y)}{\partial y} = \frac{2\pi d^*}{\Phi_0}H_x + \frac{2\pi d_1}{\Phi_0}4\pi M_{x1} + \frac{2\pi d_2}{\Phi_0}4\pi M_{x2}, \quad \text{(A4)}$$

$$\frac{\partial\varphi(x, y)}{\partial x} = \frac{2\pi d_1}{\Phi_0}4\pi M_{y1} + \frac{2\pi d_2}{\Phi_0}4\pi M_{y2}. \quad \text{(A5)}$$

Here $H_x$ is the applied magnetic field in the $x$ direction and $d_{1,2}$ are the thicknesses of $F_{1,2}$ layers. The total supercurrent $I_s = I_{ss} + I_{sl} + I_{tr}$, Eqs. (1)–(3), is integrated over the JSV area using the obtained values $\alpha(x, y)$ and $\varphi(x, y)$. To find the critical current, we maximized the supercurrent with respect to the integration constant. For more details of the simulation procedure, see Ref. [32]. In Figs. 6 and 7 we show results corresponding to one of the studied JSV's Ni(5 nm)/Cu(10 nm)/Ni(7.5 nm) with sizes $160 \times 860$ nm$^2$ [42]. Simulations are shown for the following set of supercurrent amplitudes: $I_{ss0} = 0.1$, $I_{sl0} = 1.0$, $I_{tr0} = 3.0$, which fits well the experimental data. From this we conclude that the triplet current amplitude in our JSV's is approximately three times larger than the singlet, $I_{tr0}/(I_{sl0} + I_{ss0}) \simeq 3$.

Figure 6(a) shows the magnetization curve along the easy axis (see the inset). Black lines represent the major hysteresis loop, and color lines represent FORC's with $H_{\parallel\max}$ indicated by circles. The spin valve appears to be at the border between the mono- and the two-domain states. Upon sweeping of the field upward from the saturated ↓↓ state, magnetization in the F layers first curves into a C shape (state $A$), which is reversible without hysteresis (see the green line). Then the $F_1$ and $F_2$ layers switch sequentially into the state with two domains (states $B$ and $C$) simultaneously flipping the $x$-component of magnetization. Hysteresis appears in the state $B$ (red line), which corresponds to the AP state $\langle\alpha\rangle \simeq 180°$.

Figure 6(b) shows amplitudes of the long-range singlet (blue) and triplet (red) supercurrents for an upward field sweep. In the AP state $B$, the singlet amplitude is large and the triplet is small. On both sides of it, there are two noncollinear states $A, C$ with large triplet and small singlet amplitudes. At large positive/negative fields the JSV is in the parallel state with vanishing of both long-range singlet and triplet components. The shape of the $I_c(H)$ pattern of the JSV depends on the relative amplitudes of singlet and triplet components. Figure 6(c) shows the case with the dominant triplet current ($I_{ss0} = 0.1$, $I_{sl0} = 1.0$, $I_{tr0} = 3.0$) for the total (black), singlet (blue), and triplet (red) currents. Since in this case the total current is dominated by the triplet current, $I_c(H)$ has two peaks corresponding to the noncollinear states $A$ and $C$, separated by a dip, corresponding to the AP state $B$, similar to the experimental data in Fig. 5(d).

In Figs. 6(d)–6(i) we analyze $I_c(H_\parallel)$ FORC's, corresponding to $M(H)$ curves with the same color in Fig. 6(a). Panel (d) represents the case when $H_{\parallel\max}$ is within the first $I_c(H)$ peak. Here the spin valve is in the reversible noncollinear state $A$. In (e) $H_{\parallel\max}$ is within the dip in the AP state $B$. As emphasized in the main text, the fingerprint of the AP state is the appearance of hysteresis; see the red line in Fig. 6(a).

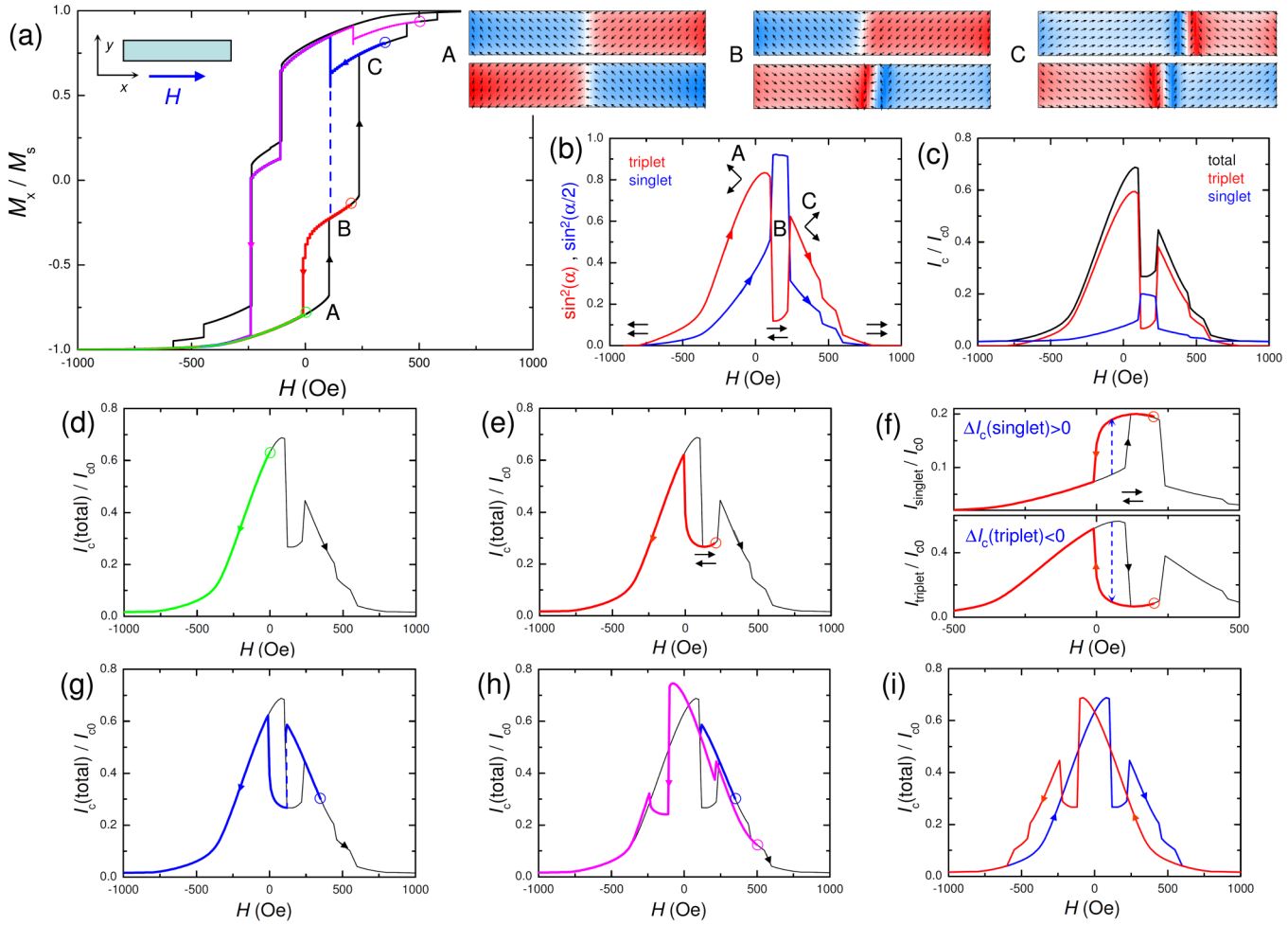


FIG. 6. Simulations for easy-axis field orientation. (a) Magnetization curves $M_x(H_x)$. Black curves represent the major hysteresis and color curves FORC's with different $H_{\parallel\max}$, indicated by circles. The top right panel shows magnetization distribution in $F_{1,2}$ layers at points $A$, $B$, and $C$. (b) Sample-averaged values of normalized triplet [$\propto \sin^2(\alpha)$, red] and singlet [$\propto \sin^2(\alpha/2)$, blue] current amplitudes for the upward field sweep. It is seen that the triplet amplitude has a minimum in the AP state-$B$, surrounded by the two maxima in the noncollinear states $A$ and $C$. The singlet current has a single maximum in the AP state-$B$. (c) Corresponding critical currents for the case when the triplet amplitude is ∼3 times larger than the singlet. (d)–(i) Simulated FORC's for the reversal curves from (a). Note that the hysteresis appears when the JSV switches into the magnetostatically stable AP state-$B$; see panel (e). Panel (f) demonstrates that in this hysteresis the singlet current is enhanced, while the triplet is reduced. Therefore, enhancement (reduction) of $I_c$ upon the appearance of the hysteresis is an unambiguous fingerprint of dominant singlet (triplet) supercurrent.

Panel (f) demonstrates that within this hysteresis, the singlet current is increased (top panel) and the triplet is decreased (bottom panel). Thus, the change of the critical current upon the appearance of hysteresis tells us about the nature of the dominant supercurrent. Since in our simulations the triplet current is dominant, there is an overall drop of $I_c$ at the hysteretic branch, as seen in Fig. 6(e). Panels (g) and (h) show FORC's after switching out of the AP state $B$ into the noncollinear state $C$ with domains. Note that along with some metastability associated with domains, in Fig. 6(h) we observe a net enhancement of the central noncollinear peak at the expense of the second peak. Finally, panel (i) shows $I_c(H)$ starting from fully saturated states. Overall, presented simulations are in good agreement with experimental data for JSV's from Fig. 5(a). Simulations reproduce both the double-peak $I_c(H_\parallel)$ patterns and the nontrivial hysteresis with reduction of $I_c$ in the AP state.

We note that we assumed that the JSV is narrow enough so that the flux quantization field is larger than the saturation field. Therefore, critical current modulation is not upset by flux quantization. However, in larger JSV's flux quantization does strongly affect the $I_c(H)$ modulation [32]. This is the main reason for the size dependence of $I_c(H)$ patterns; see Fig. 3. For long JSV's with a small $\Delta H$, the double-peak structure of $I_{tr0}(H)$ is completely masked by rapid flux-quantum oscillations, leading to an overall Fraunhofer-type modulation of $I_c(H)$.

To demonstrate this, in Fig. 7 we present simulations for the same device in the hard-axis orientation with larger $L = 860$ nm; see the sketch in Fig. 7(a). Figure 7(a) shows the large hysteresis of magnetization curve $M_y(H_y)$. Here the intermediate AP step is also present, but with a limited range of existence compared to the easy axis; see Fig. 6(a). This occurs because at $H = 0$ moments $M_{1,2}$ tend to align with the

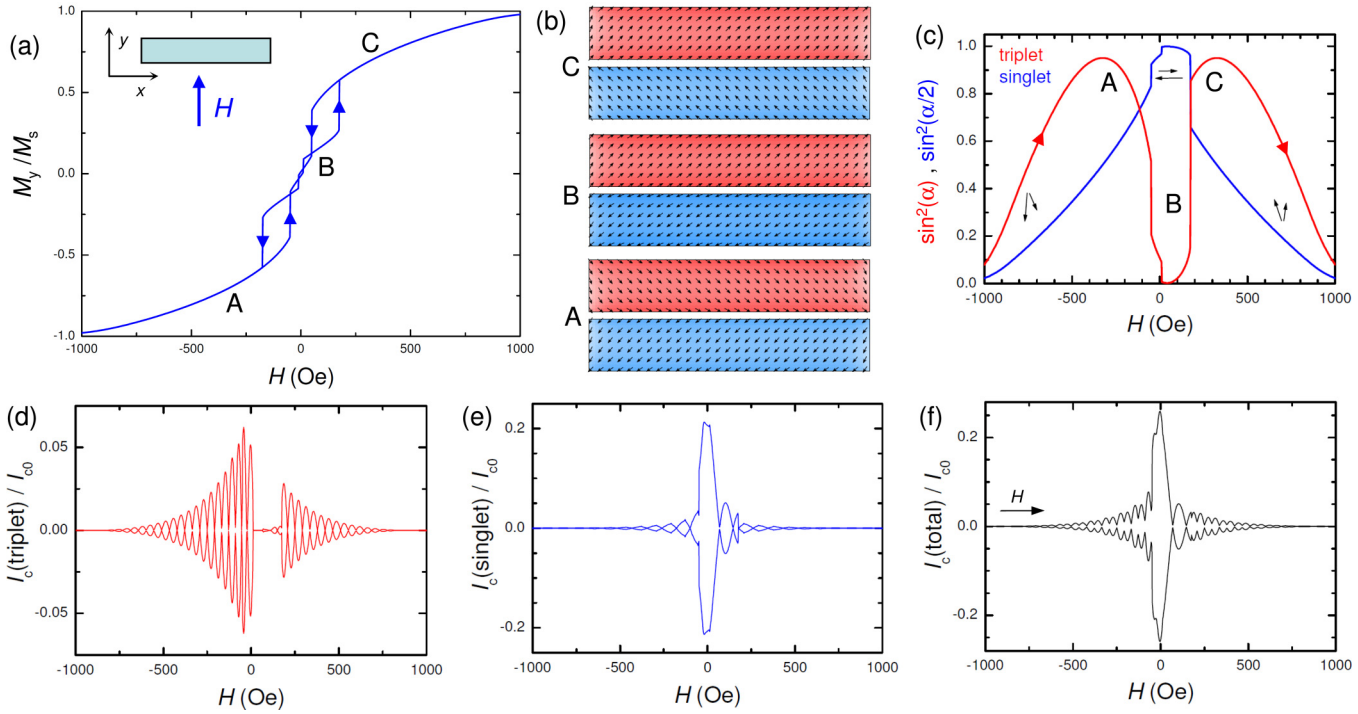


FIG. 7. Simulations for the hard-axis orientation. (a) Magnetization curves. (b) Configurations of magnetization at points $A$, $B$, and $C$. (c) Sample-averaged values of normalized triplet [$\propto \sin^2(\alpha)$, red] and singlet [$\propto \sin^2(\alpha/2)$, blue] current amplitudes for the upward field sweep. Panels (d)–(f) show magnetic field modulation patterns for (d) triplet, (e) singlet, and (f) total critical currents. It can be seen that although the triplet current amplitude in (c) has two clear peaks in noncollinear states $A, C$, the small flux quantization field at this field orientation leads to rapid damped oscillations, which suppress the triplet supercurrent (see the vertical scale). Therefore, the characteristic double-maxima become unrecognizable in the total $I_c(H)$ modulation (f). This explains how the flux quantization effect changes $I_c(H)$ patterns for JSV's from a double to a single peak for easy- and hard-axis orientations, respectively.

easy $x$-axis, destroying the AP state. To the contrary, the range of fields for coherent rotation of magnetization is broader, and both layers remain in the monodomain state. Corresponding distributions of magnetizations are shown in Fig. 7(b) for points $A$, the first noncollinear state upon coherent rotation from the negative parallel state; $B$, the antiparallel state; and $C$, the second noncollinear state upon switching from the AP state.

Figure 7(c) shows sample-averaged values of normalized triplet, $\propto \sin^2(\alpha)$ (red), and singlet, $\propto \sin^2(\alpha/2)$ (blue), current amplitudes; see Eqs. (3) and (2). The behavior of both components is similar to the easy-axis case; see Fig. 6(b). That is, in this respect the field orientation does not make any principal difference. However, the $I_c(H)$ pattern is strongly affected in this orientation. Figures 7(d)–7(f) show magnetic field modulation of (d) the triplet, (e) the singlet, and (f) the total currents. It can be seen that although the triplet current amplitude in panel (c) has two clear peaks ($A, C$), the small flux quantization field $\Delta H$ in this orientation, which is much smaller than the coercive field, significantly distorts the $I_c(H)$ pattern. At points $A$ and $C$ with the largest triplet amplitudes there are already many flux quanta inside the JSV, suppressing the triplet critical current by more than an order of magnitude. As a result, the characteristic double-maxima feature becomes unrecognizable in the total $I_c(H)$ modulation. Thus, the difference between easy- and hard-axis orientations is entirely due to the flux quantization effect. Nevertheless, both numerical simulations [see Figs. 6(b) and 7(c) and the experimental analysis in Figs. 4 and 5] demonstrate that the essential physics remains independent of the field orientation.

[1] A. I. Buzdin, Proximity effects in superconductor-ferromagnet heterostructures, Rev. Mod. Phys. **77**, 935 (2005).
[2] F. S. Bergeret, A. F. Volkov, and K. B. Efetov, Odd triplet superconductivity and related phenomena in superconductor-ferromagnet structures, Rev. Mod. Phys. **77**, 1321 (2005).
[3] Ya. V. Fominov, A. A. Golubov, T. Yu. Karminskaya, M. Yu. Kupriyanov, R. G. Deminov, and L. R. Tagirov, Superconducting triplet spin valve, JETP Lett. **91**, 308 (2010).
[4] Ya. M. Blanter and F. W. J. Hekking, Supercurrent in long SFFS junctions with antiparallel domain configuration, Phys. Rev. B **69**, 024525 (2004).
[5] M. Eschrig, Spin-polarized supercurrents for spintronics: A review of current progress, Rev. Prog. Phys. **78**, 104501 (2015).
[6] M. Houzet and A. I. Buzdin, Long range triplet Josephson effect through a ferromagnetic trilayer, Phys. Rev. B **76**, 060504 (2007).

[7] Y. Asano, Y. Sawa, Y. Tanaka, and A. A. Golubov, Odd triplet superconductivity and related phenomena in superconductor-ferromagnet structures, Phys. Rev. B **76**, 224525 (2007).

[8] L. Trifunovic, Z. Popovic, and Z. Radovic, Josephson effect and spin-triplet pairing correlations in $SF_1F_2S$ junctions, Phys. Rev. B **84**, 064511 (2011).

[9] L. Trifunovic, Long-Range Superharmonic Josephson Current, Phys. Rev. Lett. **107**, 047001 (2011).

[10] A. S. Mel'nikov, A. V. Samokhvalov, S. M. Kuznetsova, and A. I. Buzdin, Interference Phenomena and Long-Range Proximity Effect in Clean Superconductor-Ferromagnet Systems, Phys. Rev. Lett. **109**, 237006 (2012).

[11] N. G. Pugach and A. I. Buzdin, Magnetic moment manipulation by triplet Josephson current, Appl. Rev. Lett. **101**, 242602 (2012).

[12] M. Alidoust, G. Sewell, and J. Linder, Non-Fraunhofer Interference Pattern in Inhomogeneous Ferromagnetic Josephson Junctions, Phys. Rev. Lett. **108**, 037001 (2012).

[13] C. Richard, A. Buzdin, M. Houzet, and J. S. Meyer, Signatures of odd-frequency correlations in the Josephson current of superconductor/ferromagnet hybrid junctions, Phys. Rev. B **92**, 094509 (2015).

[14] S. Hikino and S. Yunoki, Magnetization induced by odd-frequency spin-triplet Cooper pairs in a Josephson junction with metallic trilayers, Phys. Rev. B **92**, 024512 (2015).

[15] J. Linder and J. W. A. Robinson, Superconducting spintronics, Nat. Phys. **11**, 307 (2015).

[16] H. Meng, J. Wu, X. Wu, M. Ren, and Y. Ren, Long-range superharmonic Josephson current and spin-triplet pairing correlations in a junction with ferromagnetic bilayers, Sci. Rep. **6**, 21308 (2016).

[17] C. Bell, G. Burnell, C. W. Leung, E. J. Tarte, D.-J. Kang, and M. G. Blamire, Controllable Josephson current through a pseudospin-valve structure, Appl. Rev. Lett. **84**, 1153 (2004).

[18] J. W. A. Robinson, G. B. Halász, A. I. Buzdin, and M. G. Blamire, Enhanced Supercurrents in Josephson Junctions Containing Nonparallel Ferromagnetic Domains, Phys. Rev. Lett. **104**, 207001 (2010).

[19] B. Baek, W. H. Rippard, S. P. Benz, S. E. Russek, and P. D. Dresselhaus, Hybrid superconducting-magnetic memory device using competing order parameters, Nat. Commun. **5**, 3888 (2014).

[20] A. Iovan, T. Golod, and V. M. Krasnov, Controllable generation of a spin-triplet supercurrent in a Josephson spin valve, Phys. Rev. B **90**, 134514 (2014).

[21] Yu. N. Khaydukov, G. A. Ovsyannikov, A. E. Sheyerman, K. Y. Constantinian, L. Mustafa, T. Keller, M. A. Uribe-Laverde, Yu. V. Kislinskii, A. V. Shadrin, A. Kalaboukhov, B. Keimer, and D. Winkler, Evidence for spin-triplet superconducting correlations in metal-oxide heterostructures with noncollinear magnetization, Phys. Rev. B **90**, 035130 (2014).

[22] J. W. A. Robinson, J. D. S. Witt, and M. G. Blamire, Controlled injection of spin-triplet supercurrents into a strong ferromagnet, Science **329**, 59 (2010).

[23] T. S. Khaire, M. A. Khasawneh, W. P. Pratt, Jr., and N. O. Birge, Observation of Spin-Triplet Superconductivity in Co-Based Josephson Junctions, Phys. Rev. Lett. **104**, 137002 (2010).

[24] N. Banerjee, J. W. A. Robinson, and M. G. Blamire, Reversible control of spin-polarized supercurrents in ferromagnetic Josephson junctions, Nat. Commun. **5**, 4771 (2014).

[25] W. M. Martinez, W. P. Pratt, Jr., and N. O. Birge, Amplitude Control of the Spin-Triplet Supercurrent in S/F/S Josephson Junctions, Phys. Rev. Lett. **116**, 077001 (2016).

[26] J. A. Glick, V. Aguilar, A. B. Gougam, B. M. Niedzielski, E. C. Gingrich, R. Loloee, W. P. Pratt, Jr., and N. O. Birge, Phase control in a spin-triplet SQUID, Sci. Adv. **4**, eaat9457 (2018).

[27] K. Lahabi, M. Amundsen, J. A. Ouassou, E. Beukers, M. Pleijster, J. Linder, P. Alkemade, and J. Aarts, Controlling supercurrents and their spatial distribution in ferromagnets, Nat. Commun. **8**, 2056 (2017).

[28] O. Vávra, R. Soni, A. Petraru, N. Himmel, I. Vávra, J. Fabian, H. Kohlstedt, and Ch. Strunk, Coexistence of tunneling magnetoresistance and Josephson effects in SFIFS junctions, AIP Adv. **7**, 025008 (2017).

[29] D. Lenk, V. I. Zdravkov, J.-M. Kehrle, G. Obermeier, A. Ullrich, R. Morari, H.-A. Krug von Nidda, C. Müller, M. Yu. Kupriyanov, A. S. Sidorenko, S. Horn, R. G. Deminov, L. R. Tagirov, and R. Tidecks, Thickness dependence of the triplet spin-valve effect in superconductor-ferromagnet-ferromagnet heterostructures, Beilstein J. Nanotechnol. **7**, 957 (2016).

[30] V. A. Oboznov, V. V. Bol'ginov, A. K. Feofanov, V. V. Ryazanov, and A. I. Buzdin, Thickness Dependence of the Josephson Ground States of Superconductor-Ferromagnet-Superconductor Junctions, Phys. Rev. Lett. **96**, 197003 (2006).

[31] M. Weides, Magnetic anisotropy in ferromagnetic Josephson junctions, Appl. Phys. Lett. **93**, 052502 (2008).

[32] A. Iovan and V. M. Krasnov, Signatures of the spin-triplet current in a Josephson spin valve: A micromagnetic analysis, Phys. Rev. B **96**, 014511 (2017).

[33] I. A. Golovchanskiy, V. V. Bol'ginov, V. S. Stolyarov, N. N. Abramov, A. Ben Hamida, O. V. Emelyanova, B. S. Stolyarov, M. Yu. Kupriyanov, A. A. Golubov, and V. V. Ryazanov, Micromagnetic modeling of critical current oscillations in magnetic Josephson junctions, Phys. Rev. B **94**, 214514 (2016).

[34] T. Golod, A. Rydh, and V. M. Krasnov, Detection of the Phase Shift from a Single Abrikosov Vortex, Phys. Rev. Lett. **104**, 227003 (2010).

[35] See Supplemental Material at http://link.aps.org/supplemental/10.1103/PhysRevResearch.2.013167 for discussion of properties of Nb/Ni/Nb SFS junctions, method of determination of the critical current and measurement of spin-valve magnetoresistance.

[36] In Fig. 2 we show data for different junctions. SFS junctions and JSV's have a strong (oscillatory decaying) dependence of $I_c$ on Ni-layer thicknesses, and $I_c$, of course, scales with the area. Therefore, at a given $T$ different junctions have different $I_c$'s. The $I_c$ can be tuned by $T$, as shown in the supplemental material [35]. In the manuscript, we have chosen optimal $T$-ranges for individual devices, corresponding to $I_c$'s of several hundreds of $\mu$A. Such data represent the most detailed and low-noise measurements. The behavior of devices does not change qualitatively within this temperature range (note that Ni has a Curie temperature of 1000 K, which is much larger that the temperature difference of a few K in the superconducting state). Essentially increasing $T$ just reduces $I_c$.

[37] V. M. Krasnov, V. A. Oboznov, and N. F. Pedersen, Fluxon dynamics in long Josephson junctions in the presence of a temperature gradient or spatial nonuniformity, Phys. Rev. B **55**, 14486 (1997).

[38] F. Béron, D. Ménard, and A. Yelon, First-order reversal curve diagrams of magnetic entities with mean interaction field: A physical analysis perspective, J. Appl. Phys. **103**, 07D908 (2008).

[39] C.-I. Dobrotă and A. Stancu, What does a first-order reversal curve diagram really mean? A study case: Array of ferromagnetic nanowires, J. Appl. Phys. **113**, 043928 (2013).

[40] R. K. Dumas, P. K. Greene, D. A. Gilbert, L. Ye, C. Zha, J. Åkerman, and K. Liu, Accessing different spin-disordered states using first-order reversal curves, Phys. Rev. B **90**, 104410 (2014).

[41] V. V. Bol'ginov, V. S. Stolyarov, D. S. Sobanin, A. L. Karpovich, and V. V. Ryazanov, Magnetic switches based on NbPdFeNb Josephson junctions with a magnetically soft ferromagnetic interlayer, JETP Lett. **95**, 366 (2012).

[42] Micromagnetic simulations in Figs. 6 and 7 are done for a spin valve $160 \times 860$ nm$^2$ in the two field orientations. The data in Figs. 6(a) and 6(b) and Figs. 7(a)–7(c) do not depend on the effective magnetic thickness $d^*$. The latter is not well known. Therefore, in calculation of $I_c(H)$ we use $d^*$ as a free parameter to fit experimental data. It appears that $d^*$ is larger by approximately a factor 3 in the hard-axis orientation. This can be attributed to the larger demagnetization factor. For the easy-axis orientation the demagnetization factor is essentially zero. But for the hard axis it should be significant (overall height is 422 nm larger that the width 160 nm). This could explain the corresponding factor 3 difference in $d^*$ due to the flux-focusing effect; see, e.g., T. Golod, O. M. Kapran, and V. M. Krasnov, Planar Superconductor-Ferromagnet-Superconductor Josephson Junctions as Scanning-Probe Sensors, Phys. Rev. Appl. **11**, 014062 (2019).